# Frost Heave Dynamics at a Single Crystal Interface

L. A. Wilen and J. G. Dash
*Physics Department, University of Washington, Seattle, Washington 98195-1560*
(Received 4 October 1994)

We study flow in a surface-melted layer of a single crystal of ice at a plane solid interface. The flow, which is induced by a temperature gradient in the melted layer, causes the ice to grow normal to the interface. The process is the basis for frost heave in frozen soils. Flow is observed in a limited range of temperatures near the melting point, implying that surface melting is absent below this range. The data are analyzed in terms of a model which allows estimates of the fluid layer thickness. The results are not consistent with interfacial melting due to purely van der Waals forces.

PACS numbers: 64.70.Dv, 68.35.Md, 83.50.Lh

Frost heave is a common phenomenon in cold climates, causing significant changes in the natural environment and placing serious limitations on the design and durability of engineered structures [1–3]. The basic process involves the stable existence of unfrozen water below the bulk melting transition, which can result from one or more causes, such as surface melting and curvature effects. In a thermal gradient this liquid will flow toward a lower temperature due to the tendency to lower its chemical potential. This flow is the cause of the dilation known as frost heave. Although frost heave is conventionally treated as if peculiar to frozen ground, it has been shown that the phenomenon may occur in any solid [4–7]. Notwithstanding its universality, many aspects are unknown, because virtually all experiments have been conducted in porous media. High area porous media are advantageous because they greatly increase the total flow rates from intrinsically slow surface transport, but their typical heterogeneity and complex geometry prevent detailed measurements of the basic surface process. Surface melting is a common mechanism allowing the stable existence of melt liquid at a flat interface. Recent experiments have examined surface melting in a variety of materials using a number of different techniques [8–18]. These studies have shown that the tendency of a material to surface melt depends on crystal orientation, purity, and surface disorder; however, very little is known about layer mobility.

This paper reports the first measurements of frost heave dynamics on the plane surface of a single crystal of ice. The dynamics are sensitive specifically to the flow properties of the quasiliquid film. The observation of flow confirms the presence of a fluid layer, but only in a restricted range of temperatures close to the bulk transition temperature $T_0$. Below a specific temperature $T'$, we observe no flow and infer the absence of any melt liquid. Measurements of flow rates permit us to estimate the film thickness. Where present, the films are much thicker than can be accounted for by surface melting controlled by dispersion forces alone.

In the experiment a temperature gradient is imposed parallel to the interface between an ice crystal and a flexible membrane. The temperature gradient produces a thermomolecular pressure gradient [4,5,7,19], which induces liquid flow in the surface-melted film toward lower temperatures. The flow rate is extremely low; hence the film thickness is essentially at its equilibrium value as determined by the local temperature. Since the equilibrium thickness decreases with temperature, by continuity, the liquid must progressively convert to ice as it moves along the interface. This causes uneven ice growth, and the development of the surface topography is impressed upon the flexible membrane. The evolution of this topography is measured by interference microscopy.

The experimental arrangement is shown in Fig. 1(a). The sample cell is a thin hollow disk, 0.8 mm thick and 19.0 mm in diameter, formed by a circular hole in a fiberglass wafer, and faced by a glass plate on the bottom and a flexible polyvinylidene chloride membrane on the top. The cell is filled with distilled deionized water via capillary tubes through the periphery; after filling, one tube is sealed off and the other remains connected to an external reservoir open to ambient pressure. The center of the cell is cooled from the bottom by a Peltier device to a temperature $T_1$ below the freezing point $T_0$, while the temperature of the periphery $T_2$ is held above $T_0$. Both temperatures can be maintained within 1 mK for periods of many days. Ice is nucleated at the center by touching the membrane with a cotton tip cooled in liquid $N_2$. The ice grows out to an equilibrium radius determined by the temperature settings. By adjusting $T_1$ and $T_2$, the radius of the ice and the radial temperature gradient at the ice-water interface can be controlled independently. The grain structure and crystal orientation of the ice are examined by polarimetry. The disk generally consists of four to eight pie-shaped single crystal domains. A typical disk is shown in Fig. 1(b).

The flow and growth measurements are determined by analysis of sequences of interference fringe patterns, taken at equally spaced time intervals. Figure 2 shows three images from one series. Each image represents a region of approximately 1.0 mm $\times$ 0.5 mm . The edge of the ice disk is visible as a bright vertical arc in the

 0031-9007/95/74(25)/5076(4)$06.00 

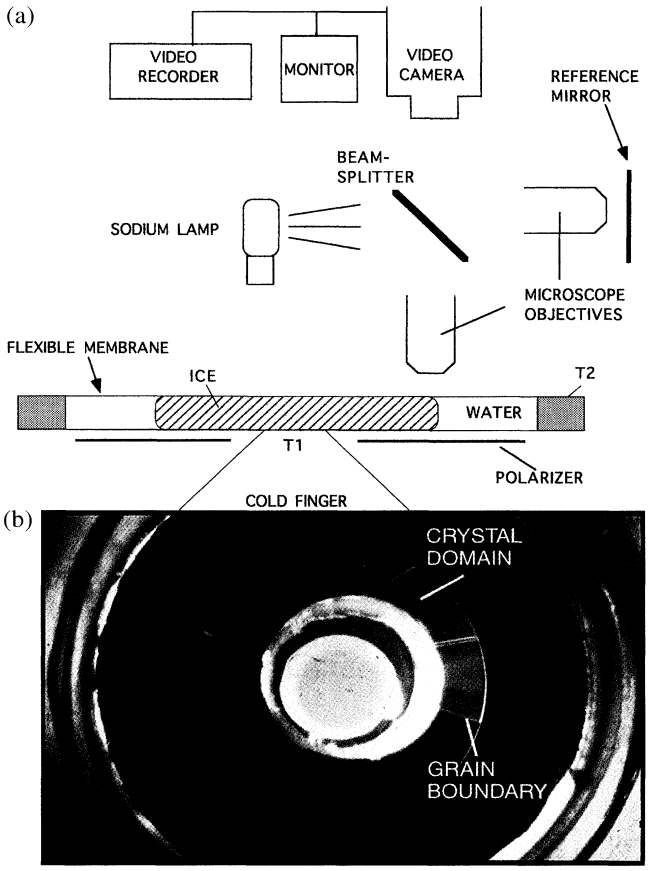


FIG. 1. (a) Experimental setup. (b) View of ice through crossed polarizers showing domain structure. Eight domains are visible.

center of each picture. A complete sequence typically consists of snapshots recorded on video at a rate of one per hour for one to two weeks. A convenient fraction of the images is digitized and analyzed to produce the membrane profiles $z(r, t)$. Figure 3 shows a typical series of profiles obtained from one run. The ice shape is assumed to be the same as the membrane shape up to within $20\mu$m of the disk edge, at which point it bends away. The pronounced ridge near the outer edge of the ice disk is due to the locally greater film thickness and flow rate near the freezing point. Continued ice growth raises the membrane which in turn presses back onto the ice, resulting in a retardation of the flow. Consequently, the observed growth rate of the ice decreases with time.

A striking feature of the data is that growth is observed at radii above a certain value $r'$, but no perceptible growth for $r < r'$. We interpret this to mean that there is surface melting at temperatures between $T_0$ and $T(r')$, but not at $T < T(r')$. Note the region of negative curvature at $r < r'$, indicating that the local pressure under the membrane is less than atmospheric. Evidently, there is sufficient adhesion to maintain contact between the

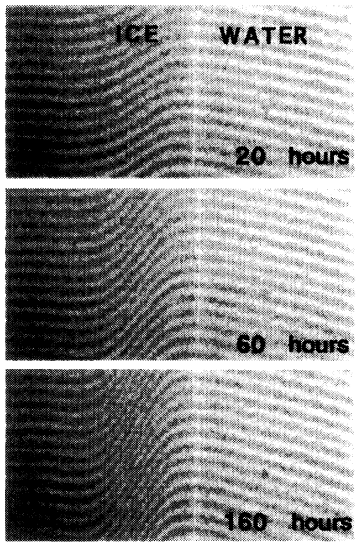


FIG. 2. Interference micrograph of membrane at three successive times, showing evolution of topology.

membrane and the ice. The profiles in Fig. 3, along with the analysis presented in the next section suggest that the film thickness drops rapidly over a narrow temperature range around $T = -0.03\,^{\circ}\mathrm{C}$.

An abrupt onset of surface melting with increasing temperature is distinct from *complete* and *incomplete* surface melting. Complete melting involves a continuous increase of film thickness with temperature, diverging as $T_0$ is approached. For incomplete melting, the thickness saturates at a finite temperature before $T_0$ is reached [20].

Each type of melting behavior corresponds to a particular functional form of the surface free energy $F(L)$. The total free energy of the film $G(L)$ is the sum of surface and bulk contributions, as

$$G(L) = F(L) + \frac{q_m(T_0 - T)}{T_0 v_i} L . \qquad (1)$$

$q_m$ is the latent heat of melting, $v_i$ is the molecular volume of ice, and $T_0$ is the melting temperature. The second term is the cost in bulk free energy for a liquid

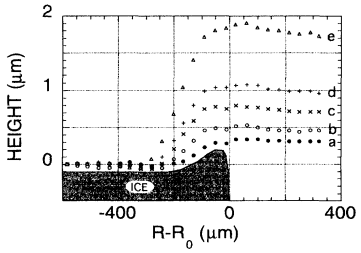


FIG. 3. Typical time series of membrane profiles. Shaded area shows inferred ice profile after 5 h. The temperature gradient in the ice at $R = R_0$ is $0.92\,^{\circ}\mathrm{C/cm}$. Curves *a* 5, *b* 20, *c* 40, *d* 60h, and *e*160 h.

film of thickness $L$ at a temperature $T$ below the melting temperature, to first order in $(T - T_0)$. The equilibrium film thickness is found by minimizing the total free energy $G(L)$. In Fig. 4(a), $F(L)$ is plotted corresponding to three different types of melting behavior. One interesting possibility, shown in the figure, is that $F(L)$ has *two* minima, with the global minimum occurring for $L \rightarrow \infty$ [21]. In this case, as the temperature is lowered, the minimum of $G(L)$ will jump discontinuously from a finite large value of $L$ to one at a small value of $L$, as seen in 4(b). Such behavior would be consistent with our data, although this is not the only form of $F(L)$ which can explain the rapid change in film thickness we observe.

$F(L)$ is the sum of all of the surface interactions present in the system. Theoretical and experimental studies have shown that one must consider van der Waals, electrical double layer, and short range interactions [22]. A detailed calculation of the van der Waals contribution to $F(L)$ for some ice/polymer interfaces [23] shows that it alone is too weak to explain the film thicknesses (discussed below) or the onset temperature observed. Electrical and short range interactions must therefore play an important role for this system. As an example, we have considered the possibility that the membrane may be partially ionized in solution with no background electrolyte [22]. Adding the electrical interaction to the van der Waals result enhances the film thicknesses in the melted region in closer agreement with the experimental results. (Conceptually, this combination is similar to that used in the theory by Derjaguin and Landau [24] and Verwey and Overbeek [25] to describe the stability of colloidal particles in solution.) The details of the jump from large to small film thicknesses depend on the exact form of the short range forces involved.

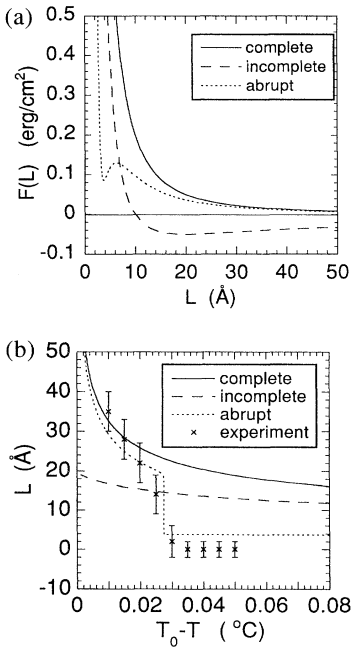


FIG. 4. (a) Excess surface free energy $F(L)$ corresponding to three types of surface melting behavior. (b) $L(T)$ calculated from curves in (a), compared with experimental values.

In the region for $r > r'$, the experimental measurements of the profile evolution can be related to physical properties of the fluid film. The following is an outline of a quantitative theory and its application to the experimental conditions. The calculation is simplified by assuming that the film is quasistatic. Hence its local thickness $L(r)$ is the equilibrium value at temperature $T(r)$.

By continuity, the velocity of the profile $z(r,t)$ is a function of time and position, according to the equation

$$\frac{\partial z(r,t)}{\partial t} = \frac{v_i}{v_w}\frac{1}{r}\frac{d}{dr}\left(r\frac{dV(r)}{dt}\right). \tag{2}$$

$dV(r)/dt$ is the volume flux for a channel of width $L$ and unit breadth, $v_w$ is equal to the molecular volume of water, and $v_i, q_m$ were defined above. Under the experimental conditions the film thickness varies very slowly; hence the flow can be treated as Poiseuille flow in a parallel sided channel. The volume flux is then given by

$$\frac{dV(r)}{dt} = \frac{L^3(r)}{12\eta(r)}\frac{dP_l(r)}{dr}, \tag{3}$$

where $dP_l(r)/dr$ is the radial pressure gradient in the liquid parallel to the interface.

The pressure in the liquid layer is derived by equating the chemical potential in the melted layer to that of the adjacent solid, and expanding about the chemical potential at a point on the solid/liquid coexistence line. Taking the gradient of both sides yields

$$\frac{dP_l(r)}{dr} = \left(\frac{v_i}{v_w}\right)\left(\frac{dP_i(r)}{dr} + \frac{q_m}{v_i T_0}\frac{dT(r)}{dr}\right). \tag{4}$$

$P_i$ is the external pressure exerted on the ice by the membrane. It depends on the surface tension $\sigma$ of the membrane and the local radius of curvature $R$, as $P_i = \sigma/R$. The second term on the right is the thermomolecular pressure gradient associated with the temperature gradient.

Equations (2), (3), and (4) fully define the evolution of the ice profile in terms of the temperature dependence of film thickness and viscosity. In one limit, the profile takes a particularly simple form. At very small times, the membrane is almost flat and the term due to the membrane pressure may be dropped. Integrating Eq. (2) with respect to $r$ and combining with Eqs. (3) and (4) then yields

$$\frac{L^3(r)}{12\eta(r)} = \frac{v_w^2 T_0}{v_i q_m}\left(\frac{dT}{dr}\right)^{-1}\frac{1}{r}\int_a^r r'dr'\frac{\partial z(r',t)}{\partial t}\bigg|_{t=0}, \tag{5}$$

where the lower limit of the integral, $a$, is a radius below which the film thickness is assumed to be negligible.

To deduce $L(T)$ from the data requires an estimate of $\eta(T)$ in the film. It is known that the viscosity of very thin films is greater than that of the bulk liquid, due to layerlike ordering at an interface (proximity effect) [26–28]. With a trial assumption that the film $\eta$ has its bulk values $\eta(T)$ [29], the calculated thicknesses are shown in Fig. 4(b).

These thicknesses are not much larger than the typical scale of the proximity effect, and hence the true viscosity is likely to be larger than the bulk viscosity. The actual thicknesses will then be greater than those calculated using the bulk value of $\eta$. At temperatures between $-0.010\,^{\circ}\mathrm{C}$ and the melting point, the flow rates are influenced by curvature effects even for very small times, and hence cannot be used to determine film properties within this approximation. Recent theoretical work has made significant progress in calculating flow rates including the effect of membrane curvature [30].

Further measurements will explore the effects of other crystal orientations and interfacial materials.

We are grateful to J. Wettlaufer and M. Schick for many stimulating discussions. This work has been supported by NSF Grants No. DPP 90-23845 and No. DMR 94-00637 and ONR Grant No. N00014-90-J-1369.

[1] A. L. Washburn, *Geocryology* (John Wiley and Sons, New York, 1980).
[2] *Permafrost, Engineering Design and Construction,* edited by G. H. Johnston (John Wiley and Sons, New York, 1981).
[3] P. B. Black and M. J. Hardenberg, Cold Regions Research and Engineering Laboratory, Hanover, NH, Report No. 90-1.
[4] B. V. Derjaguin and N. V. Churaev, Cold Regions Research and Technology **12**, 57 (1986).
[5] K. S. Førland, T. Førland, and S. K. Ratkje, *Irreversible Thermodynamics* (John Wiley and Sons, New York, 1988), pp. 235-244.
[6] M. Hiroi *et al.,* Phys. Rev. B **40**, 6581 (1989).
[7] J. G. Dash, in *Phase Transitions in Surface Films 2,* edited by H. Taub *et al.* (Plenum Press, New York, 1991), pp. 339-356; J. Low Temp. Phys. **89**, 277 (1992).
[8] M. Elbaum, S. G. Lipson, and J. G. Dash, J. Cryst. Growth **129**, 491 (1993).
[9] J. W. M. Frenken and J. F. van der Veen, Phys. Rev. Lett. **54**, 134 (1985).
[10] Y. Furukawa, M. Yamamoto, and T. Kuroda, J. Cryst. Growth **82**, 665 (1987).
[11] Y. Furukawa and I. Ishikawa, J. Cryst. Growth **128**, 1137 (1993).
[12] J. Krim, J. P. Coulomb, and J. Bouzidi, Phys. Rev. Lett. **58**, 583 (1987).
[13] D. Beaglehole and D. Nason, Surf. Sci. **96**, 363 (1980).
[14] D. Beaglehole and P. Wilson, J. Phys. Chem. **98**, 8096 (1994).
[15] D. M. Zhu and J. G. Dash, Phys. Rev. Lett. **57**, 2959 (1986).
[16] P. H. Fuoss, L. J. Norton, and S. Brennan, Phys. Rev. Lett. **60**, 2036 (1988).
[17] B. Pluis, A. van der Gon, J. W. M. Frenken, and J. F. van der Veen, Phys. Rev. Lett. **59**, 2678 (1987).
[18] R. R. Gilpin, J. Colloid Interface Sci. **77**, 435 (1980).
[19] R. R. Gilpin, Water Resources Research **16**, 918 (1980).
[20] M. Elbaum and M. Schick, Phys. Rev. Lett. **66**, 11713 (1991).
[21] L. D. Landau and E. M. Lifshitz, *Statistical Physics* (Pergamon Press, Oxford, 1980).
[22] J. Israelachvili, *Intermolecular and Surface Forces* (Academic Press Inc., London, 1992).
[23] L. A. Wilen, J. S. Wettlaufer, M. Elbaum, and M. Schick (to be published).
[24] B. V. Derjaguin and L. Landau, Acta Physicochim. URSS **14**, 633 (1941).
[25] E. J. W. Verwey and J. Th. G. Overbeek, *Theory of Stability of Lyophobic Colloids* (Elsevier, Amsterdam, 1948).
[26] J. Q. Broughton, A. Bonissent, and F. F. Abraham, J. Chem. Phys. **74**, 4029 (1981).
[27] D. M. Zhu and J. G. Dash, Phys. Rev. Lett. **60**, 432 (1988).
[28] R. Evans, Adv. Phys. **28**, 143 (1979).
[29] H. R. Pruppacher, J. Chem. Phys. **56**, 101 (1972).
[30] J. S. Wettlaufer and M. G. Worster, Phys. Rev. E **51**, 4679 (1995).

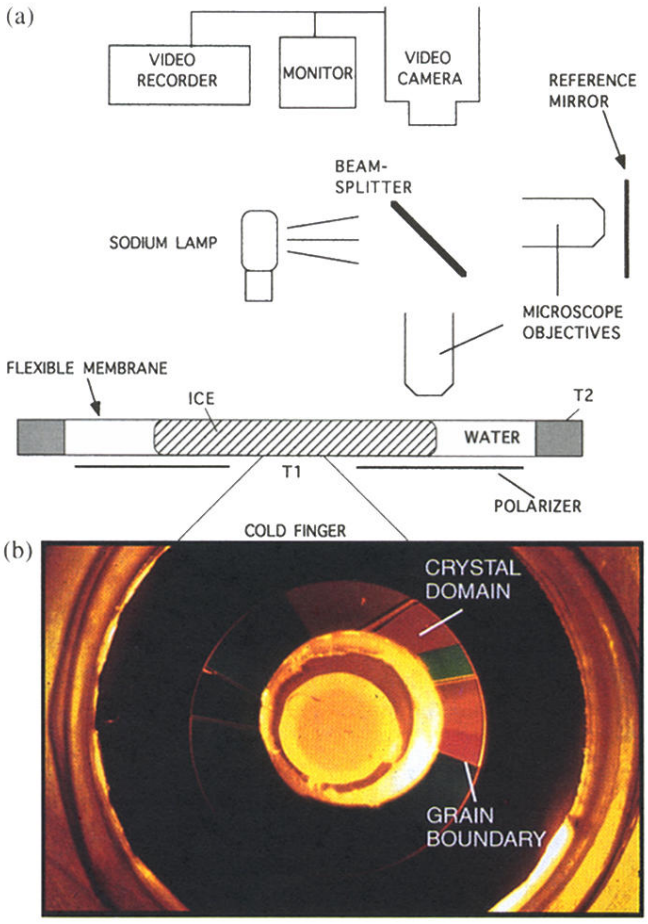


FIG. 1. (a) Experimental setup. (b) View of ice through crossed polarizers showing domain structure. Eight domains are visible.

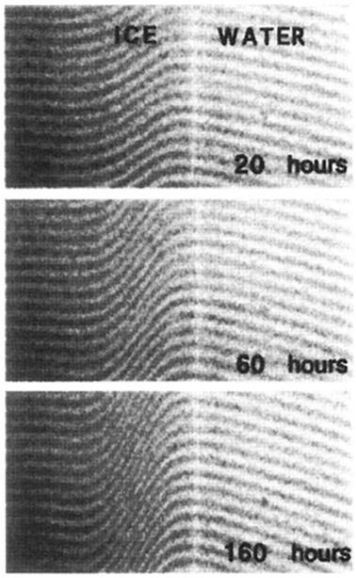


FIG. 2. Interference micrograph of membrane at three successive times, showing evolution of topology.

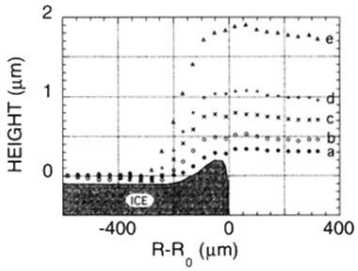


FIG. 3. Typical time series of membrane profiles. Shaded area shows inferred ice profile after 5 h. The temperature gradient in the ice at $R = R_0$ is 0.92 °C/cm. Curves *a* 5, *b* 20, *c* 40, *d* 60h, and *e*160 h.